PCCP

PAPER

View Article Online
View Journal | View Issue

Cite this: *Phys. Chem. Chem. Phys.*, 2026, **28**, 7869

Trajectory surface hopping study of photocatalyzed H_2 dissociation on a gold cluster

Prabhash Mahata and George C. Schatz *

Modelling of nonadiabatic reactions for heterogeneous photocatalysis involving absorbates on metal nanoparticles provides insight for the interpretation of experiments. In this paper, photoinduced H_2 dissociation in a Au_6H_2 model complex has been investigated using Time-Dependent Density Functional Theory (TDDFT), and with a decoherence corrected fewest switches surface hopping (DC-FSSH) approach that includes all degrees of freedom of the Au_6H_2 cluster in the photodynamics. The excited states of this cluster near the equilibrium geometry mostly involve weakly entangled combinations of transitions between occupied orbitals with 60% gold d-orbital character and unoccupied orbitals that are 95% sp, with little variation between different excited states for energies close to what is the Au plasmon energy for larger clusters. Both adiabatic and nonadiabatic process play significant roles in H–H bond dissociation, with adiabatic dissociation always being fast and nonadiabatic dissociation involving slow or fast mechanisms and little variation in the dissociation dynamics when different excited states are considered. In all cases both hydrogen atoms end up chemisorbed on the Au cluster, in contrast to earlier work which suggested that dissociation was dominated by one or both H atoms going to the gas phase. Most H–H bond dissociation reactions take place *via* the nonadiabatic pathway and leading to both hydrogens chemisorbed on the nearest Au atom, but others lead to H's on different Au atoms. H_2 desorption from the Au_6 cluster competes with hydrogen dissociation, and is always nonadiabatic for this model. Charge transfer between the adsorbed H_2 molecule and the Au_6 cluster is found to make a minor contribution to H–H dissociation. Instead, the calculations show that nonadiabatic transitions between metal localized states are dominant, and that the lowest excited metal-localized state adiabatically evolves into an H_2 dissociative state. These calculations provide new insights to an important model system for plasmon mediated photocatalysis.

Received 8th December 2025,
Accepted 5th March 2026

DOI: 10.1039/d5cp04764a

rsc.li/pccp

I. Introduction

One of the typical heterogeneous reactions on metallic surfaces[1,2] is H_2 dissociation. Usually this is a thermally induced catalytic result, but plasmon mediated H_2 dissociation on nanomaterial surfaces has been found to be very effective in several studies.[3–8] This type of photochemical reaction is enhanced by localized surface plasmon resonance (LSPR) excitation[9–12] which involves collective excitation of the conduction electrons in metals like Au, Ag, Cu and Al. Subsequent decay of the plasmon produces hot electrons (HEs), and charge transfer to nearby adsorbates that facilitates hydrogen (H_2) dissociation.[5–8,13] Many other photocatalyzed reactions have been found, including the decomposition of ammonia (NH_3),[14] carbon monoxide (CO) bond activation,[15] splitting of water (H_2O),[16–18] carbon dioxide (CO_2) reduction,[19,20] hydrogenation reactions[21] *etc*. This has led to the realization that LSPRs have important applications[22–25] in photocatalysis.

In a chemical reaction involving multiple electronic states, a key opportunity for theory is the use of nonadiabatic dynamics to simulate the dynamics responsible for reaction. Nonadiabatic reaction dynamics studies,[26–29] either with quantum molecular dynamics simulations using multi-configurational time-dependent Hartree(MCTDH) approach[30–34] or using a semiclassical method,[26,35] are limited for these applications due to available methods and computational costs. Time dependent density functional theory (TDDFT) opens opportunities for describing nonadiabatic dynamics[36] with several electronic states and the ability to treat large molecules, however for reactions on metal clusters there are still important limitations. One method for circumventing this is to use the self-consistent charge density functional tight binding (SCC-DFTB) method, which is especially efficient when done using real-time (RT) calculations in combination with classical Ehrenfest type dynamics simulations.[37] However, a limitation with this approach is that very high intensity pulsed fields are

Department of Chemistry, Northwestern University, Evanston, Illinois 60208, USA. E-mail: g-schatz@northwestern.edu

needed to achieve dissociation, which can be difficult to connect with experimental studies that are commonly done with CW irradiation.[8]

Although there have been several computational studies of photoinduced H_2 dissociation on metal nanoparticles,[6–8,38] the best choice for simulating full dimensional dynamics is not still clear. H_2 absorbed on small metal clusters will necessarily involve a large number of excited electronic states which makes surface-hopping calculations challenging, with very little previous work on this topic.[15,38] However, a well-defined dynamics study involving these model systems and how the nonadiabatic events that lead to reaction is crucial for a detailed understanding of the processes that lead to H_2 dissociation. With the aim of maximizing mechanistic insight using trajectory surface hopping (TSH), in this work we have chosen to study Au_6H_2 as a model system for describing plasmon induced H_2 dissociation. As has been noted previously,[38] this has limited number of low-lying electronic states for dynamics simulations, so although it is not large enough to demonstrate realistic plasmon effects, the energies of the lowest lying states are similar to that of the gold plasmon, and many features of the dynamics resemble what is expected for much larger Au nano clusters.[5,39]

A previous study of the same (Au_6H_2) system[38] had important limitations that we have avoided in the present study. In that work, only two coordinates were used in describing the nuclear dynamics, with all other coordinates being frozen. One coordinate was the internuclear H–H distance, and the other was the distance between the center of mass of H_2 and the nearest tip atom of the triangular-shaped Au_6 cluster. Dissociation in this model could only occur when both H atoms separated from the cluster. Although this does describe a mechanism for H_2 dissociation, a study based on RT-TDDFT[8] found that usually one H atom remains on the cluster after dissociation (and sometimes both do), and this is consistent with experimental measurements in which gold hydride was observed by infrared measurements[40] for H_2 dissociation on gold nanoparticles. We have found in the present study where all atoms are allowed to move in three dimensions that there are important changes in the reaction dynamics relative to this earlier work that influence both the results and the interpretation of the experiments. Another limitation of the earlier surface hopping work is that a two-state diabatic representation was assumed in the dynamics based on potential energy surfaces in which an adiabatic surface that showed no H–H bond dissociation was combined with one that correlates to an antibonding repulsive state of the H_2 molecule. In this picture, surface hopping always leads to dissociation, which we will find is not true in our more general description.

In the present study, we consider full TSH dynamics based on adiabatic potential surfaces and with derivative coupling driving nonadiabatic transitions. Also, the trajectories sample all initial vibrational modes of the electronic ground state based on the NEWTON-X dynamics code[26,41,42] which leads different dynamical processes in which purely adiabatic dynamics can lead to dissociation in some cases, and where nonadiabatic events do not necessarily lead to H–H bond breaking. In addition, the photoabsorption cross section has been calculated for different initial electronic states within an energy window consistent with plasmon energies in larger clusters, thus making it possible to see if the dynamics changes much for different metal excited states. Detailed investigation of H–H dissociation through each route has been discussed. In addition, the time evolution of the H_2 charge is studied to gain a better understanding of the relation between charge transfer, nonadiabatic transitions, and H–H dissociation.

This article has been organized as follows; Section II describes the electronic structure and TSH methods and computational details. Section III includes Results and Discussion. Section IV narrates the conclusions.

II. Methods and calculations

Au_6H_2 has been studied with DFT and TDDFT using the ORCA[43,44] electronic structure package. The generalized gradient approximation (GGA) PBE[45] functional with a def2-TZVP[46] basis was used for geometry optimization. PBE and other GGA functionals have often been used for metal calculations because of computational efficiency and because GGA gives a reasonable description of gold cluster ground state geometry, energy, excited state energies and photophysical properties. The Triple-Zeta Valence Polarized basis (def2-TZVP) allows us to maintain the excited state properties(energy, gradient) along with reasonable computational cost during the dynamics, so the PBE/def2-TZVP level of theory is a good choice. We also note that in a previous study[38] the same level of theory was used. The ground state optimized structure is shown in Fig. 1. The H–H bond distance is 0.79 Å and the distance from the tip of the Au_6 cluster to the center of the H–H bond is 1.9 Å which is the same as previously reported by Guo *et al.*[38] The gas phase H–H bond distance is 0.74 Å. The slightly longer H–H bond distance is due to absorption on the Au_6 surface; this type of behavior is also seen for larger gold and silver nanoparticles.[8] The vibrational frequencies are calculated for the optimized geometry in the ground electronic state, and then the NEWTON-X[41] code is used to generate coordinates for determining optical spectra, and to set

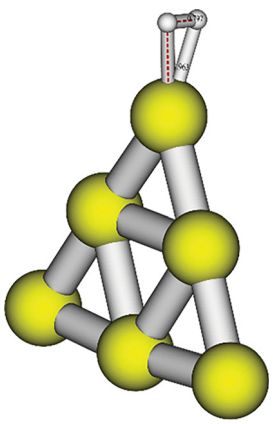

Fig. 1 Ground state optimized geometry of the Au_6H_2 complex.

up initial conditions for the trajectories. These coordinates and momenta are derived from the Wigner distribution,[47] which in the NEWTON-X[41,42] program is given for the vibrational ground state by $P_{\mathrm{w}}(\mathbf{q},\mathbf{p}) = \prod_{i=1}^{N_{\mathrm{F}}} \frac{\alpha_i}{\pi\hbar} \exp\left(-\frac{2\alpha_i}{\hbar\omega_i}\left(\frac{\mu_i\omega_i^2 q_i^2}{2} + \frac{p_i^2}{2\mu_i}\right)\right)$ where $\alpha_i = \tan h\left(\frac{\hbar\omega_i}{2k_{\mathrm{B}}T}\right)$ and at $T = 0$ K temperature $\alpha_i = 1$. A stochastic algorithm is used for sampling q and p independently, as described later. The Wigner distribution is a Gaussian function in coordinate and momentum space. An uncorrelated sampling of these two spaces has been used, with coordinate ($\mathbf{q}$) and momentum ($\mathbf{p}$) sampled randomly, with only small displacements from equilibrium involved for the Au cluster. The H_2 is also sampled from the zero point, but here the available energy is about 0.25 eV so vibrational displacements are much larger. Variation of the results with initial conditions can be seen in Fig. S1 to S4.

II.A Spectrum generation

Once we have the initial geometries, the vertical excitation energies and their corresponding oscillator strengths are calculated for each initial condition. In this study we have included the 20 lowest singlet excited states of the Au_6H_2 model system. The vertical excitation energies and their corresponding oscillator strengths for the lowest 10 excited states are shown in Table 1. It is seen that the oscillator strength for states 3 (2.48 eV) and 4 (2.62 eV) have larger values compared to other excited electronic states. In this nuclear ensemble approach the photoabsorption spectrum is generated by calculating the absorption cross section for all initial conditions derived from the Wigner distribution according to the following formula[42]

$$\sigma^{\mathrm{pa}}(E) = \frac{\pi e^2\hbar}{2m_{\mathrm{e}}c\varepsilon_0 E}\sum_{K}^{N_{\mathrm{e}}}\frac{1}{N_{\mathrm{p}}}\sum_{n}^{N_{\mathrm{p}}}\Delta E_{1K}(\boldsymbol{R}_{\mathbf{n}})f_{1K}(\boldsymbol{R}_{\mathbf{n}})g(E-\Delta E_{1K}(\boldsymbol{R}_{\mathbf{n}}),\delta)\text{-}$$

where the $\sigma^{\mathrm{pa}}(E)$ is the photoabsorption cross section at photon energy E, $\hbar$ is the reduced Planck constant, ε_0 the vacuum permittivity, c is the speed of light, e and m_{e} are electronic charge and mass. Also, there are N_{P} values of the initial coordinates $\boldsymbol{R}_{\boldsymbol{n}}$, and N_{e} values of the final excited states labeled as $K = 1, \ldots, N_{\mathrm{e}}$), while ΔE and f are the vertical excitation energy and oscillator strength, g is a normalized Gaussian that defines the lineshape function. Each geometry forms a Gaussian of width δ and an approximate absorption spectrum is achieved by averaging over all the excitations in the ensemble. The resulting spectrum spreads out quite broadly due to the randomly generated geometries in combination with several important electronic transitions.

To generate the average spectrum, we have sampled 500 initial conditions. This simulated spectrum is shown in Fig. 2. We see that there are several transitions over the range 2.0 to 3.3 eV which is quite similar to the TD-TDDFT spectrum reported by Guo[38] *et al.* The first significant peaks are around 2.47 eV, which is close to the plasmon energy in gold nanoparticles, but we discuss later that in this case the transitions are only weakly plasmonic in nature.

Table 1 Vertical excitation energies and oscillator strengths of Au_6H_2 model calculated at the PBE/def2-TZVP level of theory

Transitions	Vertical excitation energy (eV)	Oscillator strength
Ground state 1	2.2598	0.0021
Ground state 2	2.3721	0.0001
Ground state 3	2.4762	0.0615
Ground state 4	2.6194	0.0252
Ground state 5	2.832	0.0001
Ground state 6	2.9181	0
Ground state 7	2.9243	0.0003
Ground state 8	2.9342	0.0285
Ground state 9	2.9649	0
Ground state 10	2.9653	0.0005

II.B Generation of trajectories from the initial conditions:

In TSH dynamics simulations, we need the nuclear coordinates, momenta and initial electronic state from where the trajectory will commence. Among all initial conditions that were used for the spectrum simulation, we have restricted the energy window within the 2.47 ± 0.25 eV range which is the energy of the third excited state. Newton-X[41] uses a stochastic algorithm for selecting initial conditions which starts from a chosen excited state within the energy window $\varepsilon \pm \delta\varepsilon$ using the following inequality $|\Delta E_{0\mathrm{K}}(\mathbf{R}_i) - \varepsilon| \leq \delta\varepsilon$ and $r \leq \frac{f_{0\mathrm{K}}(\mathbf{R}_i)}{f^{\max}}$ where $\Delta E_{0\mathrm{K}}$ is the energy difference between ground and excited electronic state K, $f_{0\mathrm{L}}$ is the oscillator strength for this transition and $f^{\max}$ is the maximum oscillator strength for all states and among all initial conditions. The random number r is generated from a uniform distribution in the range [0,1].

We have also generated a second set of trajectories in which the dynamics simulation is started from the fourth excited state with energy in the range 2.62 ± 0.3 eV to get an idea whether the dynamics changes if we start the trajectories from a higher excited electronic state.

II.C Trajectory surface hopping dynamics simulation details

To simulate the TSH dynamics we have used the NEWTON-X[41] suite of programming in conjunction with the ORCA electronic structure program.[48]This nonadiabatic dynamics approach was performed on the basis of molecular dynamics using adiabatic potential energy surfaces between hops. Trajectory propagations were started from the third and fourth excited states. In each propagation step, potential energy, energy gradient and derivative coupling between electronic states are calculated on the fly. This methodology is similar to our previous work.[49–51] In brief, the Velocity-Verlet algorithm is used to solve Newton's equation to obtain the position of the classical nuclei as a function of time. The Butcher algorithm is used to integrate the time-dependent Schrödinger equations. TSH decisions are based on a modified version of Tully's[52] fewest switches algorithm. A simplified decay of mixing type decoherence correction[53] is implemented in NEWTON-X[41] program which is similar to that proposed by earlier by Truhlar *et al.*[54,55] to overcome the decoherence in the TSH simulation.

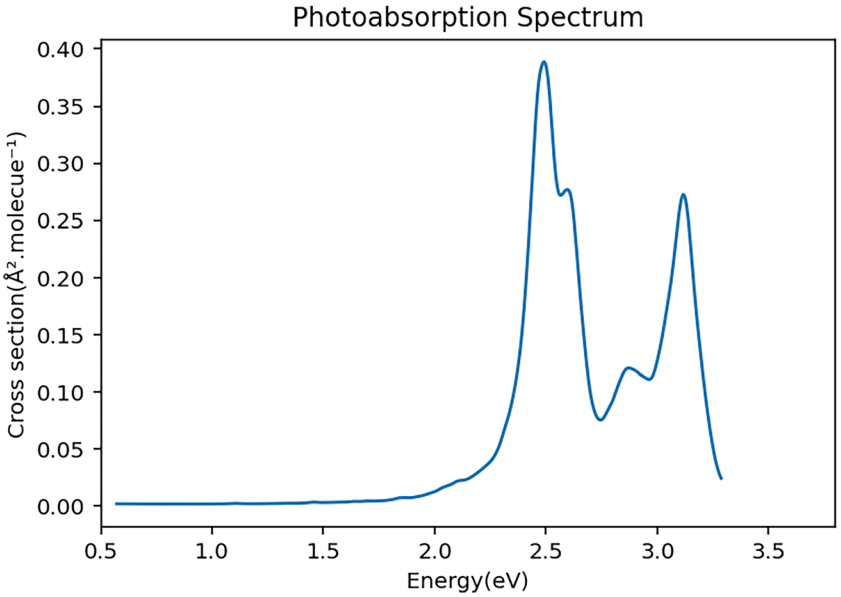

Fig. 2 Photoabsorption spectrum of Au_6H_2 calculated at PBE/def2-TZVP level of theory.

III. Results and discussion

In this study we are interested in the dissociation dynamics of H_2 absorbed at the tip of the Au_6 cluster. The trajectory analysis shows that the H_2 molecule either dissociates, or is desorbed from the Au_6 cluster surface after photoexcitation. We discuss in detail the mechanism observed for each process. We have run a batch of 226 trajectories to study the TSH dynamics on excited state 3, with each trajectory allowed to propagate a maximum of up to 1000fs. The classical trajectory propagation time is 0.5 fs which is reduced to 0.1 fs if the system's total energy is not conserved adequately. The hydrogens are either dissociated in the same electronic state from which it was started through an adiabatic process or the trajectory hops to a lower electronic state, possibly with additional hops, followed by breaking the H–H bond in a process we will call nonadiabatic dissociation.

Among the trajectories that show H-H dissociation, around 73% pass through the nonadiabatic pathway and 27% through the adiabatic pathway. Most of the adiabatic processes are fast and the H–H bond is dissociated (distance more than 2.5 Å) in less than 30 fs. The adiabatic fast dissociation does not show significant oscillations. We show one representative trajectory for adiabatic H–H bond dissociation in Fig. 3. Note that both hydrogens are bonded to the Au atom after dissociation, rather than one or both of the hydrogens being ejected into the gas phase. In this case although it takes energy to dissociate the H–H bond, some of this energy is recovered by forming two Au-H bonds. The ground state energy for this structure is 2.10 eV above the energy of the initial equilibrium geometry, and then the excited state 3 is $\sim$1 eV above that, but the initial electronic excitation energy and excitation contained in the Wigner distribution is sufficient for this to occur. We also note that this mechanism is found for all adiabatically dissociating trajectories. In the trajectory plotted in Fig. 3, the H–H bond oscillates near the tip of Au_6 surface and dissociates at around 13 fs.

In case of nonadiabatic hydrogen dissociation, the trajectories hop to lower electronic states from the initial electronic state. Here we find two types of nonadiabatic hopping trajectories, which we label "slow" and "fast" nonadiabatic hydrogen dissociation trajectories. If the effective hops occur in less than 30 fs followed by H–H dissociation, the dynamics involves fast TSH H–H dissociation. One of the representative trajectories for fast nonadiabatic hydrogen dissociation is shown in Fig. 4. The molecule hops from state 3 to state 1 at around 12 fs followed by continuous H–H bond stretching which leads to dissociation near 40 fs. In many respects, the dynamics after hopping is not significantly changed compared to that before, with only small changes in the flow of charge to the H_2 molecule, so this version of surface hopping can be considered to involve a transition between electronic states with similar properties, as would typically happen between two excited states localized on the Au_6 cluster. The slow type of nonadiabatic trajectory hops to a lower electronic state after more than 50 fs propagation time. The nonadiabatic slow dissociation process shows significant oscillations of the H–H bond. A swarm of trajectories that shows such oscillations is presented in Fig. S3. Fig. 5 shows one of these types of trajectories. The molecule stays on the same electronic state for a long propagation time followed by a hop to state 1 at around 166 fs and the full H–H bond dissociation is completed at around 250 fs. Again, we see little charge flow at the point of hopping but later the H_2 becomes slightly less positively charged and the H–H bond distance increases substantially. This suggests that when the hop takes place, the potential surface is still behaving like a metal excited state, but later there is adiabatic excitation transfer (associated with small charge transfer) leading to dissociation.

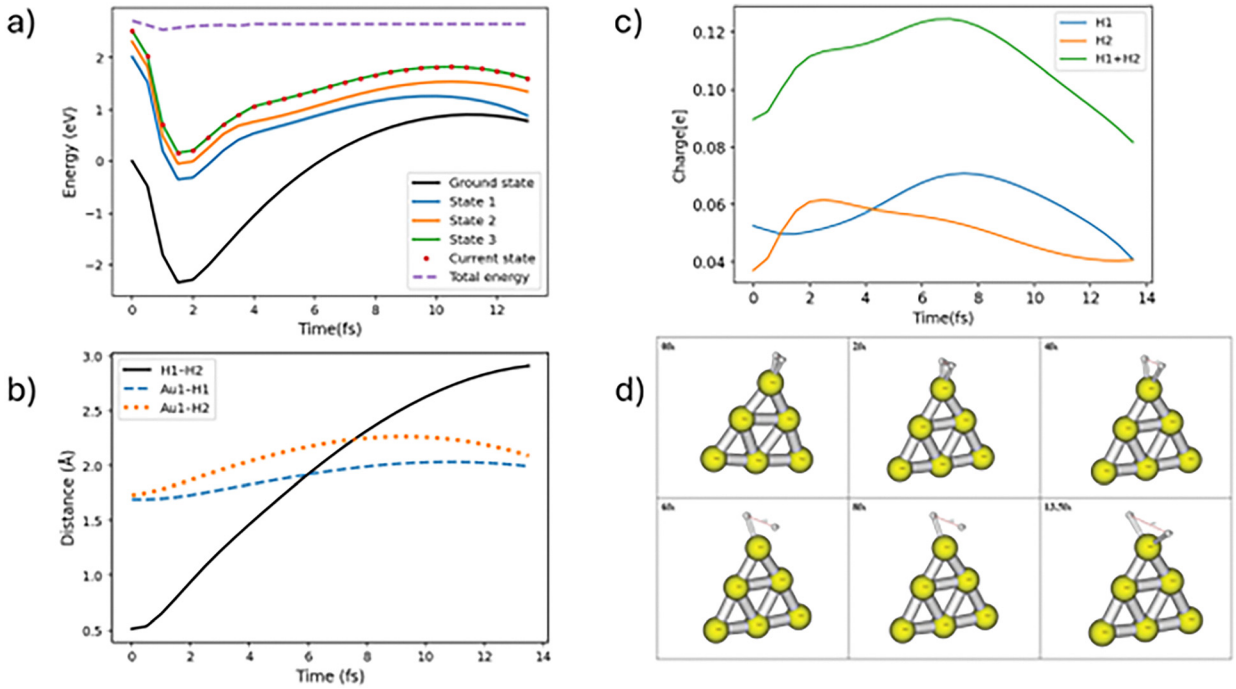

Fig. 3 Representative trajectory for adiabatic fast H_2 dissociation, leading to both H's on the same Au atom. (a) shows the four lowest singlet potential energy surfaces along with trajectory propagation time (with red dots labeling the current state of the trajectory, which takes place on excited state 3). (b) shows the change in H-H distance with time. The time evolution of Mulliken charges for H1,H2 and total charge of H_2 system is in (c). Trajectory snapshots at different time steps of the trajectory are outlined in (d).

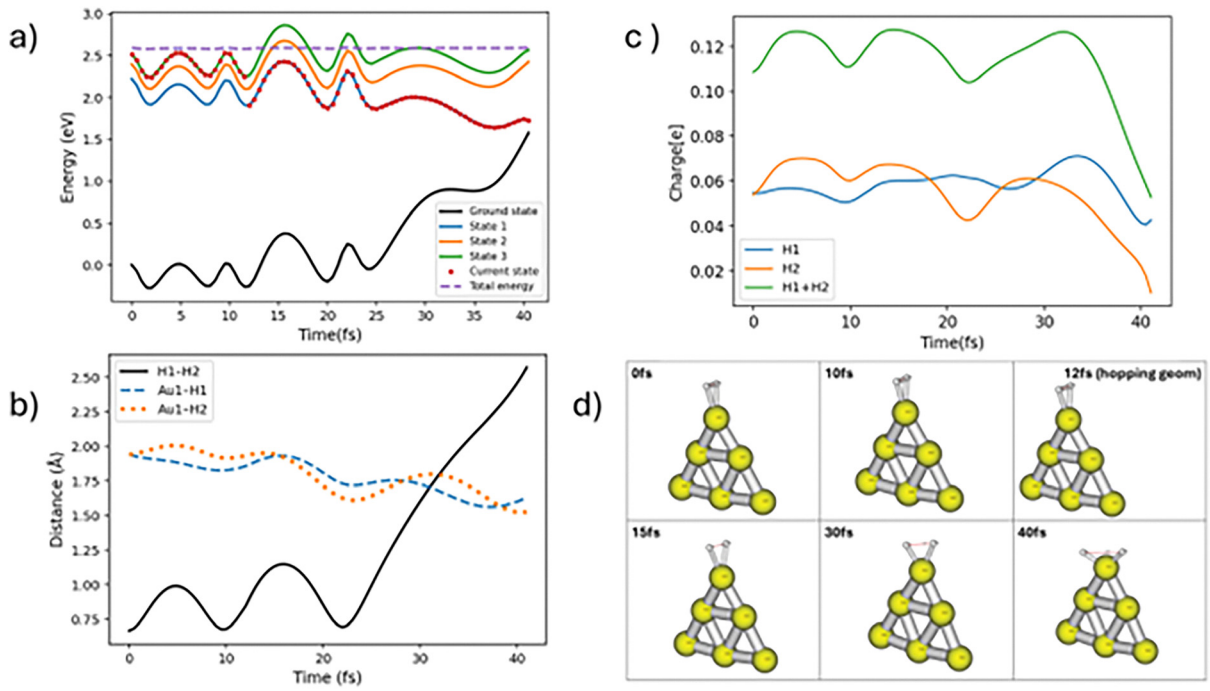

Fig. 4 Nonadiabatic trajectory for fast H–H dissociation starting in state 1. The change in potential surfaces is revealed by the red dots. Labeling of the panels is the same as in Fig. 3.

There is another mechanism for H–H bond breaking where the dissociated hydrogens end up on two different Au atoms. Note that this type of bond dissociation process occurs *via* either adiabatic or nonadiabatic processes. One of the representative trajectories has been delineated in Fig. 6. Here we see hops between states 3 and 2 near 30–60 fs that lead to more

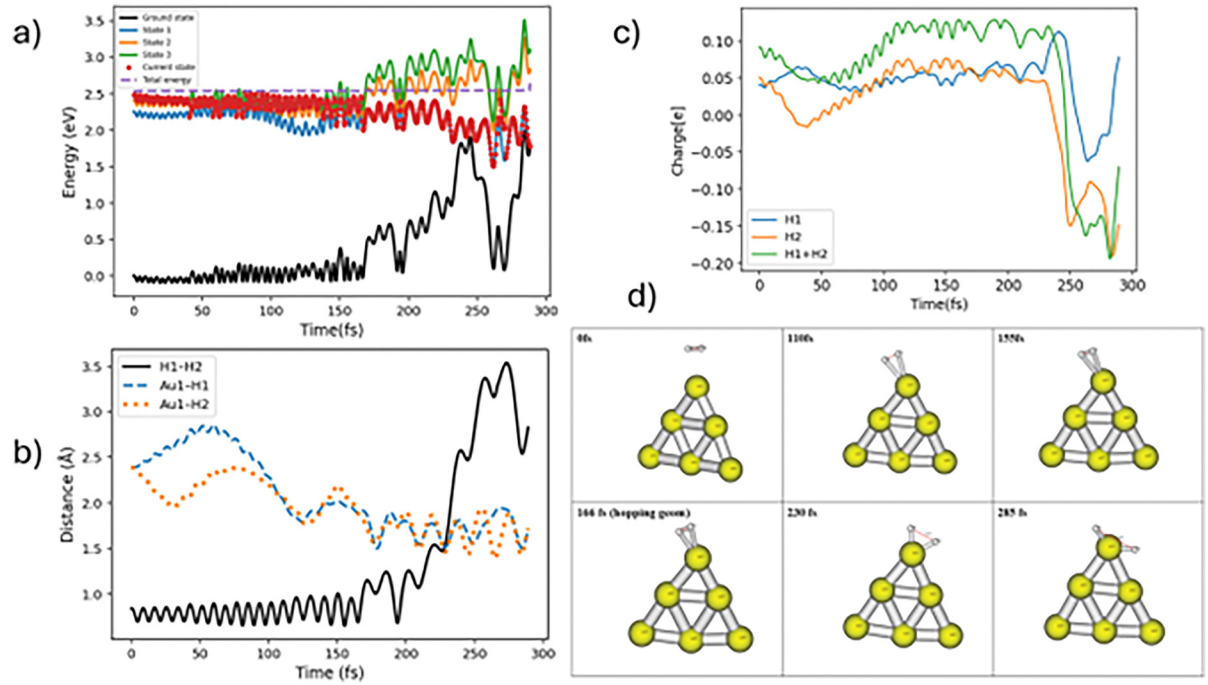

Fig. 5 Representative trajectory for nonadiabatic slow H_2 dissociation. Labeling of the panels (a)–(d) is same as in Fig. 3.

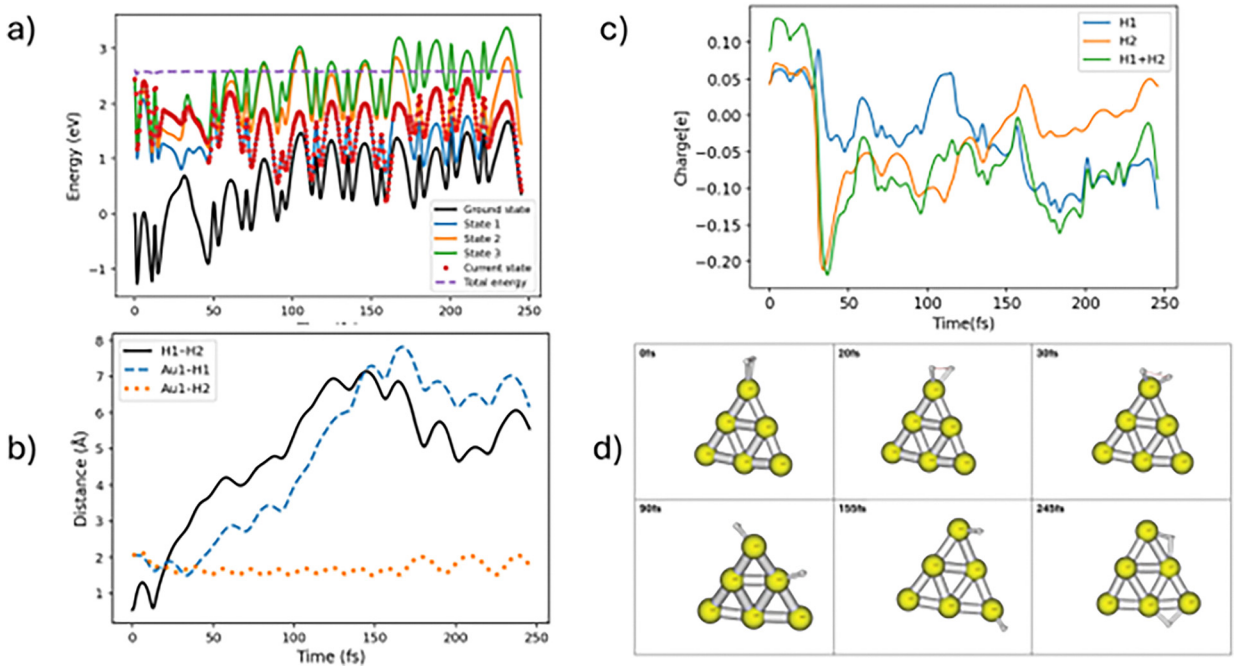

Fig. 6 Representative trajectory for H_2 nonadiabatic dissociation with H's ending up on two different Au atoms. Labeling of the panels (a)–(d) is same as in Fig. 3.

substantial charge flow to one of the H's, and subsequent H–H bond breakage. This is followed at longer times by migration of the H's to different Au atoms in what appears to be adiabatic dynamics. This trajectory shows reasonable correlation between a hop between surfaces and the flow of charge that leads to dissociation, but it isn't clear that the migration of H atoms to other gold atoms is correlated to this. Details of the charge transfer and how the wavefunction changes over time is shown in Fig. 7. This picture shows the change in HOMO/LUMO wavefunctions as well as the change in charge over time

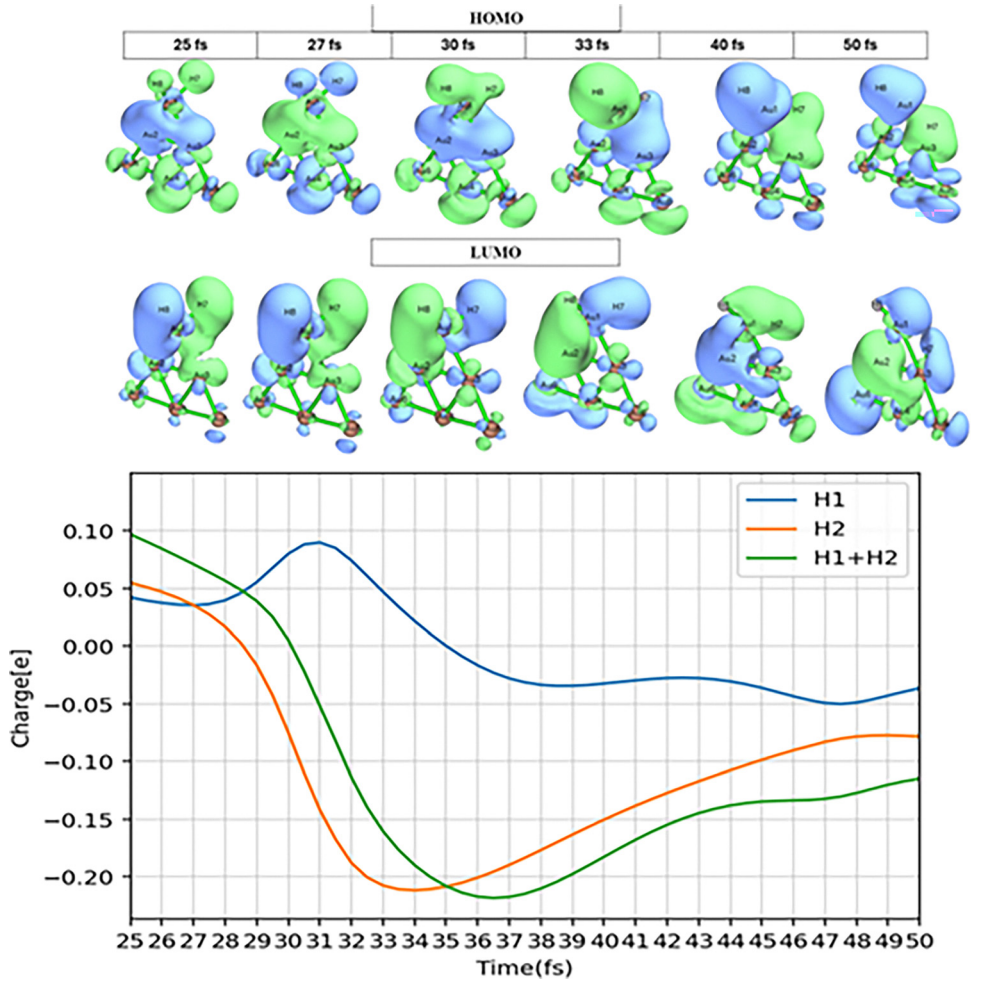

Fig. 7 Change of wavefunction (upper panel) and charge (lower panel) over time for the H–H dissociation followed by migration of one of the H atoms to a different Au atom compared to where initially it was adsorbed.

between 25 fs and 50 fs. It is clear from these panels that one of hydrogens (and eventually the other) becomes more negative at 33 fs due to charge transfer from the Au cluster to that atom. In addition, we note that the H–H bonding region shows anti-bonding character when this happens, and this leads to dissociation. Also, near 50 fs we see that some of the charge has transferred back to the Au_6, leading to gold hydrides that are more neutral in character. This nicely illustrates transient negative ion formation that has been discussed in earlier studies.[5]

Our TSH dynamics analysis also reveals that H_2 desorption also takes place from the gold cluster. In this case the H_2 molecule oscillates near the tip of the Au_6 surface, and hopping is followed by desorption. Here we assume that a trajectory leads to desorption when the distance between the center of mass of H–H and the tip Au_6 is more than 8 Å. Significantly we find that H_2 desorption is always driven by electronic transitions. In other words, energy flows from the Au_6 electronic excitation to kinetic and potential energy that ultimately leads to H_2 desorption. We also see that there is relatively short time between hops in the TSH calculations. This makes sense for transitions between metal excited states given that they are closely spaced and have similar properties, as this can lead to high probabilities for hopping. Overall, we find that H_2 desorption competes favorably with H–H bond dissociation, corresponding to around 60% of the total number of trajectories.

We have also analyzed another set of trajectory results where the dynamics started from state 4. A batch of 169 trajectories was initiated in state 4 and allowed to run to a maximum of 1000 fs. Analysis of these trajectories reveals that the H–H bond dissociation and desorption processes have similar mechanisms to those mentioned above with initial state 3. Both adiabatic and nonadiabatic dynamics contribute to H–H dissociation. Around 60% of the trajectories yield H_2 desorption and this only occurs after hops to lower states. The rest of the trajectories produced gold hydride by H–H dissociation. The fact that both states 3 and 4 lead to the same results is consistent with the orbital character of these states, as both involve similar fractions of sp and d character for the Au_6H_2 equilibrium geometry. A Natural Transition Orbital (NTO) analysis for both these states reveals both states 3 and 4

involved entangled combinations of occupied to unoccupied transitions involving the same orbitals, with the occupied orbitals involving 35% and 65% sp and d character respectively while the unoccupied orbitals are 95% sp and around 5% d character. The similar properties of these states explain why the dissociation dynamics is also similar. The entanglements are also similar, involving approximately an 80% contribution of the dominant excitation and 20% of the next most important. This indicates relatively weak entanglement, which is consistent with the weak plasmonic properties expected for this small cluster.

As the initial conditions were prepared according to a Wigner distributions using 3N-6 normal modes (N = 8 atoms), the Au–Au distances vary with time. But since we are only sampling zero point energies in the initial vibrational states, and the fastest Au-Au modes have periods of $\sim$100 fs, we find that there is no significant change in these coordinates on the time scale of H–H dissociation. Therefore, in this study H–H dissociation was not significantly influenced by any particular Au mode. Experimental studies of thermal heating effects for plasmon-driven chemistry have found only minor increases in temperature during these experiments, so the role of gold vibrational excitation is not considered to be a significant factor.[56]

IV. Conclusions

A nonadiabatic TSH study of the model system Au_6H_2 using TDDFT and the NEWTON-X surface hopping level of theory has been presented in this article. The trajectory analysis reveals that starting in electronic states with about 2.5 eV excitation leads to H–H bond dissociation with nonadiabatic as well as adiabatic pathways playing significant roles. In the case of nonadiabatic H-H dissociation the trajectories either hop to a lower electronic state in less than 30 fs (fast hopping trajectories) or they propagate on higher electronic states followed by hopping to the lowest excited electronic state in more than 50 fs. Adiabatic dissociation can also occur, and it is always fast, in many respects similar to fast nonadiabatic dissociation where the latter involves excited states where there is no significant charge transfer. Small amounts of charge transfer can take place, such as in the slow nonadiabatic charge transfer case, however charge transfer doesn't play a major role for most trajectories. Most of the trajectories involve the formation of two Au-H bonds after dissociation, where the gold atom involved is the closest to where the H_2 is initially located. However, we also found hydrogen dissociation dynamics in which the H atoms migrate to other Au atoms to form Au–H bonds. No gas phase H atoms are produced in this study, and we note that in calculations where we froze the Au_6 cluster structure (but not the H_2) during the calculations, we obtained trajectories that very closely reproduce what we obtained for the completely unfrozen structure for trajectories that are a few oscillation periods of H_2, but are only the same for a statistical ensemble when it takes longer for dissociation or desorption to occur. This indicates that the zero point energy in the Wigner distribution of Au vibrational states has little influence on the dynamics.

The results for these full dimensional calculations differ significantly from those previously reported by Zhang and coworkers[38] in that the Zhang work always associated H–H dissociation with nonadiabatic charge transfer, and a limitation of the model was that the resulting H atoms were ejected into the gas phase, rather than forming bonds to gold. This latter result is important to the interpretation of the Halas *et al.* experiments[5] as it means that the photocatalysis always leads to gold hydride formation rather an hydrogen atoms in solution. This is consistent with experimental results from Borguet[40] who observed Au–H formation using infrared measurements. Thus, in spite of the simplicity of this model, with only weak plasmonic character found in a study of the orbital character of the states using a Natural Transition Orbital analysis, the results have many features that resemble what is known about H_2 dissociation on gold nanoparticles.

Conflicts of interest

The authors declare no competing financial interest.

Data availability

All calculations in this paper have been done using the two public domain codes ORCA and Newton-X. Parameters for the calculations are described in the text, and standard input options to ORCA and Newton-X can be used to generate all the data presented. The authors will share results by reasonable request to the senior author.

Supplementary information (SI): internuclear H1–H2 distances over time for swarms of trajectories. See DOI: https://doi.org/10.1039/d5cp04764a.

Acknowledgements

This research was supported by the Division of Chemistry of the National Science Foundation under grant CHE-2347622. Support for the computational resources and staff contributions were provided for the Quest high performance computing facility at Northwestern University which is jointly supported by the Office of the Provost, the Office for Research, and Northwestern University Information Technology.

References

1 R. Van Lent, S. V. Auras, K. Cao, A. J. Walsh, M. A. Gleeson and L. B. Juurlink, Site-specific reactivity of molecules with surface defects—the case of H2 dissociation on Pt, *Science*, 2019, **363**(6423), 155–157.

2 C. Díaz, E. Pijper, R. Olsen, H. F. Busnengo, D. Auerbach and G. Kroes, Chemically accurate simulation of a

prototypical surface reaction: H2 dissociation on Cu (111), *Science*, 2009, **326**(5954), 832–834.
3 F. Libisch, J. Cheng and E. A. Carter, Electron-transfer-induced dissociation of H2 on gold nanoparticles: Excited-state potential energy surfaces via embedded correlated wavefunction theory, *Z. Phys. Chem.*, 2013, **227**(11), 1455–1466.
4 Y. Zhang, T. Nelson, S. Tretiak, H. Guo and G. C. Schatz, Plasmonic hot-carrier-mediated tunable photochemical reactions, *ACS Nano*, 2018, **12**(8), 8415–8422.
5 S. Mukherjee, F. Libisch, N. Large, O. Neumann, L. V. Brown, J. Cheng, J. B. Lassiter, E. A. Carter, P. Nordlander and N. J. Halas, Hot electrons do the impossible: plasmon-induced dissociation of H2 on Au, *Nano Lett.*, 2013, **13**(1), 240–247.
6 M. Kar and G. C. Schatz, Mechanistic Insights into the H2 Dissociation on Plasmonic Au Nanoparticles: Effect of Nanoparticle Structure and Pulse Properties on Charge-Driven Energy Transfer and Dissociation Efficiency, *J. Phys. Chem. C*, 2025, **129**(3), 1758–1768, DOI: 10.1021/acs.jpcc.4c08242.
7 N. S. Chellam and G. C. Schatz, Density Functional Tight-Binding Captures Plasmon-Driven H2 Dissociation on Al Nanocrystals, *J. Phys. Chem. C*, 2025, **129**(18), 8634–8644, DOI: 10.1021/acs.jpcc.5c00805.
8 S. K. Giri and G. C. Schatz, Photodissociation of H2 on Ag and Au Nanoparticles: Effect of Size and Plasmon versus Interband Transitions on Threshold Intensities for Dissociation, *J. Phys. Chem. C*, 2023, **127**(8), 4115–4123, DOI: 10.1021/acs.jpcc.3c00006.
9 K. L. Kelly, E. Coronado, L. L. Zhao and G. C. Schatz, The optical properties of metal nanoparticles: the influence of size, shape, and dielectric environment, *J. Phys. Chem. B*, 2003, **107**(3), 668–677.
10 K. M. Mayer and J. H. Hafner, Localized surface plasmon resonance sensors, *Chem. Rev.*, 2011, **111**(6), 3828–3857.
11 K. A. Willets and R. P. Van Duyne, Localized surface plasmon resonance spectroscopy and sensing, *Annu. Rev. Phys. Chem.*, 2007, **58**(1), 267–297.
12 E. Hutter and J. H. Fendler, Exploitation of localized surface plasmon resonance, *Adv. Mater.*, 2004, **16**(19), 1685–1706.
13 L. Zhou, C. Zhang, M. J. McClain, A. Manjavacas, C. M. Krauter, S. Tian, F. Berg, H. O. Everitt, E. A. Carter and P. Nordlander, Aluminum nanocrystals as a plasmonic photocatalyst for hydrogen dissociation, *Nano Lett.*, 2016, **16**(2), 1478–1484.
14 L. Zhou, D. F. Swearer, C. Zhang, H. Robatjazi, H. Zhao, L. Henderson, L. Dong, P. Christopher, E. A. Carter and P. Nordlander, Quantifying hot carrier and thermal contributions in plasmonic photocatalysis, *Science*, 2018, **362**(6410), 69–72.
15 X. Wu, T. van der Heide, S. Wen, T. Frauenheim, S. Tretiak, C. Yam and Y. Zhang, Molecular dynamics study of plasmon-mediated chemical transformations, *Chem. Sci.*, 2023, **14**(18), 4714–4723, DOI: 10.1039/D2SC06648C.
16 L. Yan, F. Wang and S. Meng, Quantum mode selectivity of plasmon-induced water splitting on gold nanoparticles, *ACS Nano*, 2016, **10**(5), 5452–5458.
17 S. Mubeen, J. Lee, N. Singh, S. Krämer, G. D. Stucky and M. Moskovits, An autonomous photosynthetic device in which all charge carriers derive from surface plasmons, *Nat. Nanotechnol.*, 2013, **8**(4), 247–251.
18 L. Mascaretti, A. Dutta, Š. Kment, V. M. Shalaev, A. Boltasseva, R. Zbořil and A. Naldoni, Plasmon-enhanced photoelectrochemical water splitting for efficient renewable energy storage, *Adv. Mater.*, 2019, **31**(31), 1805513.
19 G. Kumari, X. Zhang, D. Devasia, J. Heo and P. K. Jain, Watching visible light-driven CO2 reduction on a plasmonic nanoparticle catalyst, *ACS Nano*, 2018, **12**(8), 8330–8340.
20 S. Yu and P. K. Jain, The chemical potential of plasmonic excitations, *Angew. Chem., Int. Ed.*, 2020, **59**(5), 2085–2088.
21 X. Zhang, X. Li, D. Zhang, N. Q. Su, W. Yang, H. O. Everitt and J. Liu, Product selectivity in plasmonic photocatalysis for carbon dioxide hydrogenation, *Nat. Commun.*, 2017, **8**(1), 14542.
22 K. Marchuk and K. A. Willets, Localized surface plasmons and hot electrons, *Chem. Phys.*, 2014, **445**, 95–104.
23 D. Wang, W. Wang, M. P. Knudson, G. C. Schatz and T. W. Odom, Structural engineering in plasmon nanolasers, *Chem. Rev.*, 2017, **118**(6), 2865–2881.
24 Y. Zhang, S. He, W. Guo, Y. Hu, J. Huang, J. R. Mulcahy and W. D. Wei, Surface-plasmon-driven hot electron photochemistry, *Chem. Rev.*, 2017, **118**(6), 2927–2954.
25 J. Langer, D. Jimenez de Aberasturi, J. Aizpurua, R. A. Alvarez-Puebla, B. Auguié, J. J. Baumberg, G. C. Bazan, S. E. Bell, A. Boisen and A. G. Brolo, Present and future of surface-enhanced Raman scattering, *ACS nano*, 2019, **14**(1), 28–117.
26 R. Crespo-Otero and M. Barbatti, Recent Advances and Perspectives on Nonadiabatic Mixed Quantum–Classical Dynamics, *Chem. Rev.*, 2018, **118**(15), 7026–7068, DOI: 10.1021/acs.chemrev.7b00577.
27 D. R. Yarkony, Nonadiabatic Quantum Chemistry—Past, Present, and Future, *Chem. Rev.*, 2012, **112**(1), 481–498, DOI: 10.1021/cr2001299.
28 J. C. Tully, Perspective: Nonadiabatic dynamics theory, *J. Chem. Phys.*, 2012, **137**(22), 22A301, DOI: 10.1063/1.4757762.
29 G. A. Worth, M. A. Robb and B. Lasorne, Solving the time-dependent Schrödinger equation for nuclear motion in one step: direct dynamics of non-adiabatic systems, *Mol. Phys.*, 2008, **106**(16–18), 2077–2091, DOI: 10.1080/00268970802172503.
30 G. A. Worth and H.-D. Meyer, Multidimensional dynamics involving a conical intersection: wavepacket calculations using the mctdh method, *Conical Intersections*, 2004, **583–617**.
31 H.-D. Meyer; F. Gatti and G. A. Worth, *Multidimensional quantum dynamics: MCTDH theory and applications*, John Wiley & Sons, 2009.
32 H. Wang, Multilayer Multiconfiguration Time-Dependent Hartree Theory, *J. Phys. Chem. A*, 2015, **119**(29), 7951–7965, DOI: 10.1021/acs.jpca.5b03256.
33 H. Wang and M. Thoss, Multilayer formulation of the multiconfiguration time-dependent Hartree theory, *J. Chem. Phys.*, 2003, **119**(3), 1289–1299, DOI: 10.1063/1.1580111.

34 H. D. Meyer, U. Manthe and L. S. Cederbaum, The multi-configurational time-dependent Hartree approach, *Chem. Phys. Lett.*, 1990, **165**(1), 73–78, DOI: 10.1016/0009-2614(90)87014-I.
35 B. F. E. Curchod and T. J. Martínez, Ab Initio Nonadiabatic Quantum Molecular Dynamics, *Chem. Rev.*, 2018, **118**(7), 3305–3336, DOI: 10.1021/acs.chemrev.7b00423.
36 B. F. E. Curchod, U. Rothlisberger and I. Tavernelli, Trajectory-Based Nonadiabatic Dynamics with Time-Dependent Density Functional Theory, *ChemPhysChem*, 2013, **14**(7), 1314–1340, DOI: 10.1002/cphc.201200941.
37 B. Hourahine, B. Aradi, V. Blum, F. Bonafé, A. Buccheri, C. Camacho, C. Cevallos, M. Y. Deshaye, T. Dumitrică and A. Dominguez, *et al.*, DFTB +, a software package for efficient approximate density functional theory based atomistic simulations, *J. Chem. Phys.*, 2020, **152**(12), 124101, DOI: 10.1063/1.5143190.
38 Q. Wu, L. Zhou, G. C. Schatz, Y. Zhang and H. Guo, Mechanistic Insights into Photocatalyzed H2 Dissociation on Au Clusters, *J. Am. Chem. Soc.*, 2020, **142**(30), 13090–13101, DOI: 10.1021/jacs.0c04491.
39 J. C. Idrobo, W. Walkosz, S. F. Yip, S. Öğüt, J. Wang and J. Jellinek, Static polarizabilities and optical absorption spectra of gold clusters (Au n, n= 2–14 and 20) from first principles, *Phys. Rev. B:Condens. Matter Mater. Phys.*, 2007, **76**(20), 205422.
40 D. Sil, C. Lane, E. Glor, K. D. Gilroy, S. Sylla, B. Barbiellini, R. Markiewicz, M. Hajfathalian, S. Neretina and A. Bansil, *et al.*, Synthesis and Properties of Au Hydride, *ChemistrySelect*, 2019, **4**(14), 4287–4292, DOI: 10.1002/slct.201900925.
41 M. Barbatti, M. Bondanza, R. Crespo-Otero, B. Demoulin, P. O. Dral, G. Granucci, F. Kossoski, H. Lischka, B. Mennucci and S. Mukherjee, *et al.*, Newton-X Platform: New Software Developments for Surface Hopping and Nuclear Ensembles, *J. Chem. Theory Comput.*, 2022, **18**(11), 6851–6865, DOI: 10.1021/acs.jctc.2c00804.
42 R. Crespo-Otero and M. Barbatti, Spectrum simulation and decomposition with nuclear ensemble: formal derivation and application to benzene, furan and 2-phenylfuran, *Theor. Chem. Acc.*, 2012, **131**(6), 1237, DOI: 10.1007/s00214-012-1237-4.
43 F. Neese, The ORCA program system, *WIREs Comput. Mol. Sci.*, 2012, **2**(1), 73–78, DOI: 10.1002/wcms.81.
44 F. Neese, Software update: The ORCA program system---Version 5.0, *WIREs Comput. Mol. Sci.*, 2022, **12**(5), e1606, DOI: 10.1002/wcms.1606.
45 J. P. Perdew, K. Burke and M. Ernzerhof, Generalized Gradient Approximation Made Simple, *Phys. Rev. Lett.*, 1996, **77**(18), 3865–3868, DOI: 10.1103/PhysRevLett.77.3865.
46 F. Weigend and R. Ahlrichs, Balanced basis sets of split valence, triple zeta valence and quadruple zeta valence quality for H to Rn: Design and assessment of accuracy, *Phys. Chem. Chem. Phys.*, 2005, **7**(18), 3297–3305, DOI: 10.1039/B508541A.
47 R. Schinke, *Photodissociation dynamics: spectroscopy and fragmentation of small polyatomic molecules*, Cambridge university press, 1995.
48 F. Neese, F. Wennmohs, U. Becker and C. Riplinger, The ORCA quantum chemistry program package, *J. Chem. Phys.*, 2020, **152**(22), 224108, DOI: 10.1063/5.0004608.
49 M. Ziółkowski, A. Vikár, M. L. Mayes, Á. Bencsura, G. Lendvay and G. C. Schatz, Modeling the electron-impact dissociation of methane, *J. Chem. Phys.*, 2012, **137**, 22.
50 P. Mahata and B. Maiti, Photodissociation Dynamics of Methyl Hydroperoxide at 193 nm: A Trajectory Surface-Hopping Study, *J. Phys. Chem. A*, 2021, **125**(48), 10321–10329, DOI: 10.1021/acs.jpca.1c07785.
51 P. Mahata, A. K. Rauta and B. Maiti, Trajectory surface-hopping study of 1-pyrazoline photodissociation dynamics, *J. Chem. Phys.*, 2022, **157**(19), 194302, DOI: 10.1063/5.0114698.
52 S. Hammes-Schiffer and J. C. Tully, Proton transfer in solution: Molecular dynamics with quantum transitions, *J. Chem. Phys.*, 1994, **101**(6), 4657–4667, DOI: 10.1063/1.467455.
53 G. Granucci and M. Persico, Critical appraisal of the fewest switches algorithm for surface hopping, *J. Chem. Phys.*, 2007, **126**(13), 134114, DOI: 10.1063/1.2715585.
54 M. D. Hack and D. G. Truhlar, A natural decay of mixing algorithm for non-Born–Oppenheimer trajectories, *J. Chem. Phys.*, 2001, **114**(21), 9305–9314, DOI: 10.1063/1.1368388.
55 C. Zhu, S. Nangia, A. W. Jasper and D. G. Truhlar, Coherent switching with decay of mixing: An improved treatment of electronic coherence for non-Born–Oppenheimer trajectories, *J. Chem. Phys.*, 2004, **121**(16), 7658–7670, DOI: 10.1063/1.1793991.
56 E. L. Keller and R. R. Frontiera, Ultrafast Nanoscale Raman Thermometry Proves Heating Is Not a Primary Mechanism for Plasmon-Driven Photocatalysis, *ACS Nano*, 2018, **12**(6), 5848–5855, DOI: 10.1021/acsnano.8b01809.

